A Multiparcel Model for Shallow Cumulus Convection

R. A. J. NEGGERS AND A. P. SIEBESMA

Royal Netherlands Meteorological Institute, De Bilt, Netherlands

H. J. J. JONKER

Department of Applied Physics, Thermo-fluids Section, Delft University of Technology, Delft, Netherlands

(Manuscript received 10 March 2000, in final form 11 October 2001)

ABSTRACT

A new parameterization for cumulus convection is formulated, that consists of an ensemble of small, rising parcels. Large eddy simulation (LES) results are used to parameterize the lateral mixing of such a parcel: for the mixing process a relaxation timescale is defined and its value is determined by investigating individual LES clouds. The timescale is found to be nearly independent of cloud depth, which implies that the entrainment rate is inversely proportional to the vertical velocity. As a consequence, a dynamical feedback mechanism is established: the parcel dynamics influence the mixing rate, which, together with the environmental properties, feeds back on the parcel properties and therefore on the parcel dynamics.

The multiparcel model is validated with LES fields. The characteristics of the buoyant part of the clouds are reproduced: the decreasing fractional cover and increasing liquid water content with height, the vertical dynamics and mass flux, and the conserved properties and the marginally buoyant state. The model also produces the variability typical for shallow cumulus.

1. Introduction

Turbulent mixing between a cumulus cloud ensemble and its environment has been recognized as a key issue for understanding the dynamics of cumulus convection already since the work of Stommel (1947). However, the coexistence of a wide range of models, each emphasizing different aspects of the mixing mechanism, indicates that there is still no consensus on the principal mixing mechanism for turbulence in cumulus clouds (for a review see Blyth 1993; Siebesma 1998). The early cloud models, developed in the sixties (Squires and Turner 1962; Simpson et al. 1965; Simpson and Wiggert 1969; Simpson 1971), essentially consisted of a rising parcel that is diluted by environmental air through *lateral* mixing. But a fundamental problem was pointed out already by Warner (1970). Comparison of a lateral entraining cloud model with cloud measurements showed that it was impossible to simulate both the liquid water content and cloud-top height for individual cumulus clouds. A second problem is the observation of strong random fluctuations of liquid water, temperature, and vertical velocity in the cloud with no systematic variations from cloud edges toward the middle (Warner 1977; Jonas 1990). This is difficult to explain with a simple lateral entraining cloud model alone.

Not only the dynamics of individual clouds, but also the modeling of a whole cumulus cloud ensemble has always received great interest because of the use in parameterizations of cumulus convection in General Circulation Models (GCM). Recently, results from large eddy simulations (LES) of nonprecipitating shallow cumulus convection have been reported (Siebesma and Holtslag 1996) that suggest that vertical transport of heat and moisture by a shallow cumulus ensemble can be described by a simple lateral entraining bulk model, *provided* that the appropriate value for the lateral mixing rate is used. Several authors (Nordeng 1994; Grant and Brown 1999) have formulated new parameterizations in order to estimate the mixing rate for the whole cloud ensemble. However, the typical variability of temperature, moisture, and vertical velocity as observed in cumulus cloud ensembles can never be properly understood on the basis of a single pragmatic bulk model. This variability is an essential variable in statistical cloud schemes for GCMs (e.g., Cuijpers and Bechtold 1995), which are based on the idea presented by Sommeria and Deardorff (1977).

These problems have led to the formulation of a class of models that we will refer to as *stochastic* mixing models. The essence of these models is that a cloud or cloud ensemble is represented by an ensemble of air

Corresponding author address: Dr. R. A. Neggers, Royal Netherlands Meteorological Institute, P.O. Box 201, AE De Bilt 3730, Netherlands.
E-mail: neggers@knmi.nl

parcels, each having a different mixing fraction with environmental air. The major problem in stochastic modeling is how to define the distribution of these mixing rates in the ensemble. A lack of suitable observations of mixing in cumulus clouds that could be used as a critical test, has caused a divergence in the formulation of these stochastic mixing models (Emanuel 1991; Raymond and Blyth 1986; Kain and Fritsch 1990; Hu 1997).

This study is an attempt to use LES results instead to formulate an expression for the lateral mixing rate of a small updraft parcel as a function of its own properties and of those of the environment it interacts with. Then, as a test of this new parcel model, a distribution of buoyant cloud parcels is released from cloud base in an attempt to reproduce the typical variability observed in cumulus convection. The parcel ensemble will be initialized on and evaluated against 3D LES fields. In previous multiparcel methods, observational cloud data were used for validation purposes.

More specifically, the model should be able to reproduce some well established properties of the dynamics of a shallow cumulus ensemble such as produced by LES: 1) the monotonically decreasing cloud cover with height; 2) the temperature, specific humidity, and vertical velocity profiles; 3) the bulk value of the lateral mixing rate of the cloud ensemble; and 4) the variances and covariances of temperature, specific humidity, and vertical velocity of the cloud ensemble. In section 2 the motivation for this study is further discussed using a conserved variable diagram. In section 3 the single parcel model will be described and discussed, and the method of validation will be presented in section 4. Results of the multiparcel test are compared with LES results in section 5. Finally conclusions and perspectives will be given in section 6.

2. Conserved variable diagrams

The direct motivation for this study is given by a conserved variable diagram, also called a Paluch diagram (Paluch 1979). In these diagrams, the liquid potential temperature θ_l is plotted against the total specific humidity q_t. These thermodynamic variables are conserved for phase changes in shallow nonprecipitating cumulus; they can only change by mixing with air of different q_t and θ_l. Therefore these diagrams characterize the mixing processes in a shallow cumulus cloud ensemble. Figure 1 is an example of such a diagram for the 1260-m-level of a cloud ensemble produced by LES of the Barbados Oceanographic and Meteorological Experiment (BOMEX; for a description see appendix A). The vertical profile of the horizontal mean values is also plotted. The top left end of this profile represents the relatively moist and cool subcloud layer, and the warm and dry inversion is positioned in the lower right corner. The conditionally unstable cloud layer stretches in between. The diamonds represent the values of the gridpoints at the 1260-m level. The saturation curve and zero buoyancy line of this height are also plotted, dividing the figure into four sectors. All points above the saturation line represent the clouds, and the so-called cloud core is defined as the group of points in the saturated, buoyant sector.

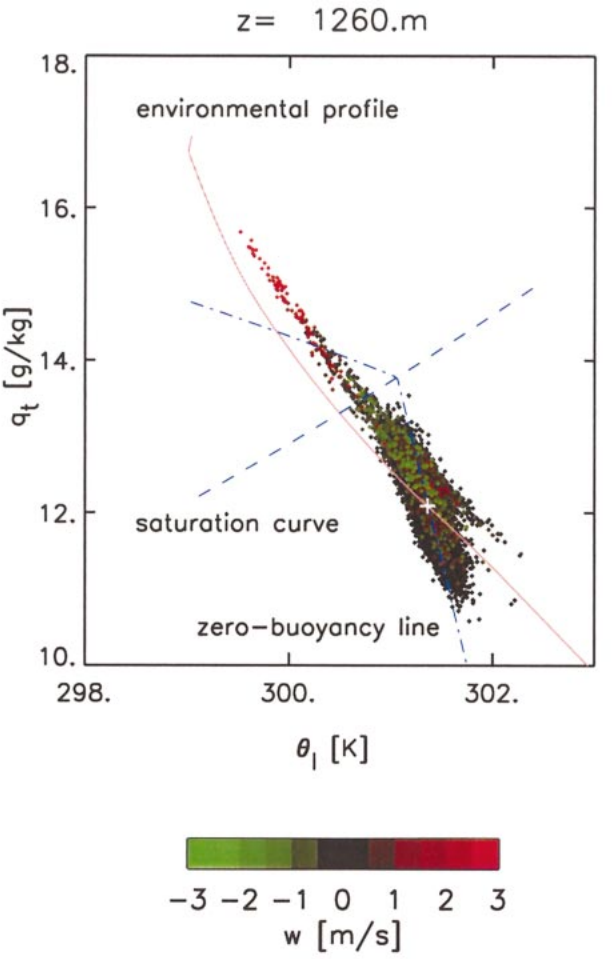

FIG. 1. A conserved variable diagram for the BOMEX case of θ_l and q_t as produced by LES. All grid boxes at 1260 m height are plotted as diamonds. The vertical velocity of each point is indicated by their color, ranging from green (descent) via black (no motion) to red (ascent). The solid orange line is the vertical profile of the horizontal mean values of q_t and θ_l, of which the values at 1260 m are indicated by the cross. The dashed blue line indicates the saturation curve, and the dash-dotted blue line indicates the zero-buoyancy line at that height.

What immediately catches the eye is the ''tail'' formed by the cloudy points, and the diffusive ''blob'' around the environmental averages. It demonstrates that the distributions of the conserved variables of the cloud ensemble are highly correlated. This is the strong fingerprint of the mixing processes in the cumulus ensemble. Note that both the highest vertical velocities and the largest excess values of θ_l and q_t are found in the cloud core. This illustrates that the cloud core is responsible for most of the vertical transport of the conserved variables in a cumulus cloud field, as was shown

by Siebesma and Cuijpers (1995). The various intercomparison studies of the Global Energy and Water Experiment (GEWEX) Cloud System Studies (GCSS) Working Group I on shallow cumulus (Siebesma et al. 2001, manuscript submitted to *J. Atmos. Sci.*; Stevens et al. 2001; Brown et al. 2001) illustrate that there is concensus about this in the LES community.

The precise nature of the responsible mixing mechanism has been the subject of many studies in the past. Early analyses of sailplane measurements inside developing cumuli congestus (Paluch 1979), gave similar results as the one presented in Fig. 1: the cloud data are scattered fairly well on a straight between cloud base and a point (the so-called source of entrainment) well above the level of observation. These results were interpreted as empirical evidence for vertical mixing of undiluted air from cloud base with environmental air near cloud top through penetrative downdrafts. Since Paluch (1979), numerous studies have been reported that used the same analysis to infer the source of entrainment, with rather ambiguous conclusions. Some studies claimed that the source of entrained air originated near the cloud top (Lamontagne and Telford 1983; Austin 1985; Jensen et al. 1985; Pontikis et al. 1987), but also entrainment sources were reported near the observation level (Raymond and Wilkening 1982; Boatman and Auer 1983; Blyth et al. 1988). In most cases the source level was less than 1 km from the level of observation.

A more refined view was put forward by Blyth et al. (1988) that favors a picture of the top of a cloud that consists of an undiluted rising core with a toroidal circulation. This advancing cloud top is inducing mechanically forced downdrafts of the environmental air that is mixed with the core slightly below the advancing top. The resulting mixed parcels have a reduced buoyancy and are left behind in a trailing wake. With this mechanism the mixed air at each level consists of two-point mixture of cloud base air (the undiluted core) and environmental air slightly above the level of observation, in agreement with the observed mixing line. The weak point of this proposed mechanism is that only undiluted cloud air from the cloud base mixes with the environmental air. Indeed it is true that undiluted air has been found at all levels within cumulus clouds (Heymsfield et al. 1978; Jensen et al. 1985) but this air represents only a small fraction of the cloud. It is then difficult to understand how only this small undiluted core region participates in all mixing events with the environment. Also Fig. 1 does not support such a mechanism since most of the cloudy updraft points are diluted.

Although the interpretation of straight lines as two-point mixing process is tempting due to its simplicity, one should be cautious with it. In a recent study by Lin and Arakawa (1997), an analysis on the output of a 2D cloud-resolving model has been applied. If the data points in a cloud are plotted in a conserved variable diagram they are distributed on a quasi-straight line that intersects the sounding close to the level of observation. At first sight one might interpret this as a two-point mixing of cloud base air with environmental air near the observation level. However, by calculating the backward trajectories it was shown that the cloud air originated from *multiple* levels, all *below* the level of observation. These findings coincide with a mechanism put forward by Taylor and Baker (1991) in which, following Blyth et al. (1988), an active cumulus cloud can still be viewed as a rising thermal with a *lateral entraining ascending cloud top.* However, the condition that only undiluted air rises and mixes with the environment is relaxed. Instead, the rising thermal exists of different mixtures, ranging from the most buoyant undiluted parcels to nearly zero buoyant mixtures. Only when a mixture becomes negatively buoyant will it decelerate, stay behind, and eventually detrain by evaporation.

This mechanism is supported by kinematic observations. Aircraft observations of trade wind cumulus bands off the coast of Hawaii were analyzed by Raga et al. (1990). For active clouds below the inversion they found that vertical velocities were almost exclusively positive. Only above the inversion were equally strong downdrafts observed. Similar results were found by Jonas (1990), who studied small maritime cumulus clouds over the North Sea. Traverses through active cumuli showed organized updrafts in the clouds with only a thin shell of downdrafts of around 2 m s^{-1} outside the clouds. The values of θ_l and q_t in the downdrafts were not too different from the far field values at the observation heights. This led to the conclusion that the descent around the cloud edges is due to mechanical forcing rather than penetrative downdrafts driven by evaporative cooling. These results are supported by numerical simulations of Klaassen and Clark (1985).

Such an *intermittent entraining thermal* does not suffer from the Warner paradox (Warner 1970) since the cloud top is determined by the undiluted parcels while other parcels dilute the cloud by lateral entrainment. It is qualitatively in agreement with the observed kinematics.

The existing conceptual mixing models are of very diverse nature, ranging from lateral mixing models (Arakawa and Schubert 1974; Tiedtke 1989; Kain and Fritsch 1990; Hu 1997) to episodic/cloud-top mixing models (Emanuel 1991; Raymond and Blyth 1986). One particularly interesting class for modeling intermittently entraining thermals is formed by the *stochastic* models (Raymond and Blyth 1986; Kain and Fritsch 1990; Emanuel 1991; Hu 1997). The main concept of models of this type is the use of a whole distribution of small elements (parcels) with slightly differing properties. With such a distribution it is possible to reproduce the intermittency.

Our aim in this paper is to set up a simple multiparcel model of such an intermittent entraining thermal as described above, and to test whether it can reproduce the variability of the joint distributions of temperature,

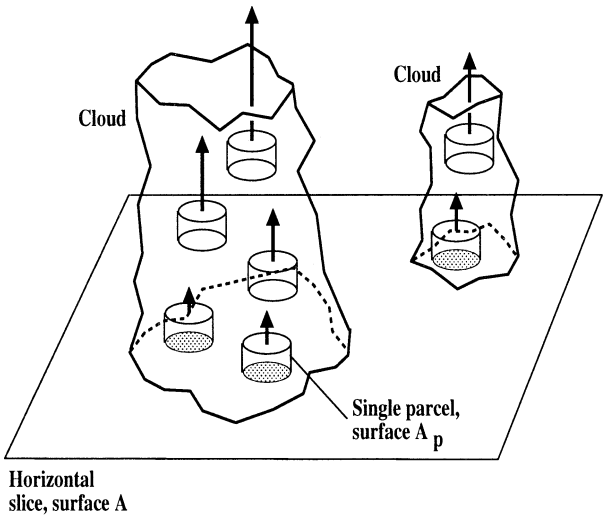

FIG. 2. A multiparcel view on shallow cumulus clouds. A cloud is considered as a group of rising parcels, visualized as cylinders with a shaded horizontal surface A_p.

moisture, and vertical velocity such as displayed in Fig. 1. The buoyant part of the cloud ensemble is modeled by releasing an ensemble of parcels. This requires knowledge of the mixing rate between such a parcel and its environment. In the next section we will present an attempt to find an expression for the mixing rate of an individual, small updraft parcel inside a cloud.

3. The parcel model

a. Governing equations

Consider a parcel as a small constant volume of air with a *fixed* horizontal area A_p and *fixed* infinitesimal thickness *dz*, see Fig. 2. Air is allowed to flow across its boundaries. The thermodynamic state of this parcel is described by the liquid water potential temperature θ_l, the total water specific humidity q_t, and the vertical velocity *w*. All other variables of interest such as the potential temperature θ, the virtual potential temperature θ_v, liquid water content q_l, and specific humidity q_v can all be derived from the moist conserved variables θ_l and q_t.

The dynamics of any field $\phi \in (\theta_l, q_t, w)$ can be written as

$$\frac{\partial \phi}{\partial t} + \nabla_h \cdot \mathbf{u}_h \phi + \frac{\partial w \phi}{\partial z} = F_\phi, \tag{1}$$

where $\mathbf{u}_h$ is horizontal velocity, ∇_h is the horizontal divergence operator, and F_ϕ contains all the sources and sinks of the field ϕ. The average value of any property of the parcel is defined as

$$\overline{(..)}^p = (..)_p \equiv \frac{1}{A_p} \int \int_{A_p} (..)\, dx\, dy \tag{2}$$

and its boundary value as

$$\overline{(..)}^b = (..)_b \equiv \frac{1}{L_b} \oint_{L_b} (..)\, dl, \tag{3}$$

where L_b denotes the length of the perimeter of the parcel. Averaging (1) over the area A_p, which is taken constant with height and time; using Gauss theorem; and assuming steady state gives

$$\frac{1}{l}\overline{u\phi}^p + \frac{\partial \overline{w\phi}^p}{\partial z} = F_{\phi,p}, \tag{4}$$

where l^{-1} is the ratio L_b/A_p, and u_b is the lateral velocity component at the boundary of the parcel, which is positive if the velocity is pointed outward. With $\phi = 1$ and no forcing, (1) becomes the continuity equation and (4) reduces to

$$\frac{1}{l}u_b + \frac{\partial w_p}{\partial z} = 0. \tag{5}$$

Applying Reynolds averaging to the fluxes

$$\overline{w\phi}^p = \overline{w'\phi'}^p + w_p \phi_p \tag{6}$$

$$\overline{u\phi}^b = \overline{u''\phi''}^b + u_b \phi_b \tag{7}$$

and substituting (5)–(7) into (4) gives

$$(\phi_p - \phi_b)\frac{\partial w_p}{\partial z} + \frac{1}{l}\overline{u''\phi''}^b + w_p \frac{\partial \phi_p}{\partial z} + \frac{\partial \overline{w'\phi'}^p}{\partial z} = F_{\phi,p}. \tag{8}$$

I II III IV V

This budget equation forms the starting point of the model.

The left-hand side of (8) consists of four terms. Term I stands for lateral inflow through the parcel's boundary due to its vertical acceleration. Term II represents the lateral turbulent mixing across the boundary. Term III is the vertical advection of parcel-mean properties, and finally term IV represents the vertical turbulent mixing within the parcel. In both terms I and II the subscript *b* emerges, representing an average over the parcel's lateral boundary. In order to obtain a closed set of equations from (8) in terms of parcel-averaged variables only, these boundary fields and boundary fluxes need to be parameterized. This requires detailed knowledge of the interaction (mixing) between the parcel and its environment.

b. Parameterizing the mixing terms using LES

Finding the mixing rate between cumulus clouds and the air surrounding them is one of the major issues in parameterizing cumulus convection, and various parameterizations have been formulated (Nordeng 1994; Siebesma 1998; Grant and Brown 1999; Gregory 2001). Direct cloud measurements of lateral mixing in clouds are difficult to realize and therefore very scarce. On cloud entrainment there is essentially only the results of Raga et al. (1990), who estimated the order of mag-

nitude of the entrainment rate. In the last decades large eddy simulation models have become an alternative tool to study cumulus convection (Sommeria 1976; Beniston and Sommeria 1981; Cuijpers and Duynkerke 1993). To evaluate the mixing terms in this parcel model, LES results on shallow cumulus are used, such as observed during BOMEX and the Small Cumulus Micro-physics Study (SCMS). For details of these cases and the LES runs see appendix A. Equation (8) will be treated term by term to determine which are dominating and which can be neglected.

First, the turbulent flux term IV in (8) is considered. Since we are dealing with small, rising parcels we can safely make the well-known top-hat approximation for the vertical flux in (6), so that term IV can be neglected.

Second, terms I and II have to be treated. The parcel is to describe an in-cloud volume of air much smaller than the typical dimensions of shallow cumulus clouds. To parameterize the mixing process in terms of parcel mean and environmental properties, the characteristics of the air that this small in-cloud parcel entrains should be specified. To this purpose LES cannot yet be used, because the typical present-day horizontal resolution of LES is too low to adequately resolve the small fluctuations inside individual cumulus clouds. This also makes it difficult to determine which of the two terms I and II is dominating in the mixing process.

To solve these problems, a more indirect method is applied, without exactly specifying the properties of the air that a parcel entrains. Observational data of the conserved thermodynamic variables inside clouds obtained from horizontal aircraft trajectories (see, e.g., Warner 1977; Jonas 1990) do show a well-defined top-hat anomaly from the environment with many perturbations around it, as visualized Fig. 3. These perturbations represent the turbulent mixing of air throughout the cloud. Although representing different processes, the mixing terms I and II both involve a combination of a velocity scale, a $\Delta\phi$ scale, and a length scale. We therefore parameterize both terms with a single expression, in the form of a relaxation term,

$$\left[(\phi_p - \phi_b)\frac{\partial w_p}{\partial z} + \frac{1}{l}\overline{u''\phi''}^{b}\right] \simeq -\frac{1}{\tau_p}(\phi_p - \overline{\phi}). \quad (9)$$

This dilution timescale τ_p is assumed to be proportional to the eddy turnover time (Siebesma 1998), which is the ratio of a vertical length scale and a velocity scale.

Ideally we would like to determine these scales using cloud observations, but as mentioned before, LES results on shallow cumulus are used instead, which are resolved well. For that reason we define some particular scales of whole cloud that are also applicable to a small in-cloud parcel. For the length-scale we take the depth of the cumulus cloud h_c in which the updraft parcel resides (see Fig. 3). This is a measure of the vertical distance that such a parcel could rise. For the velocity scale we take the cloud-averaged maximum vertical velocity $w_{\max,c}$, corrected for its cloud base velocity:

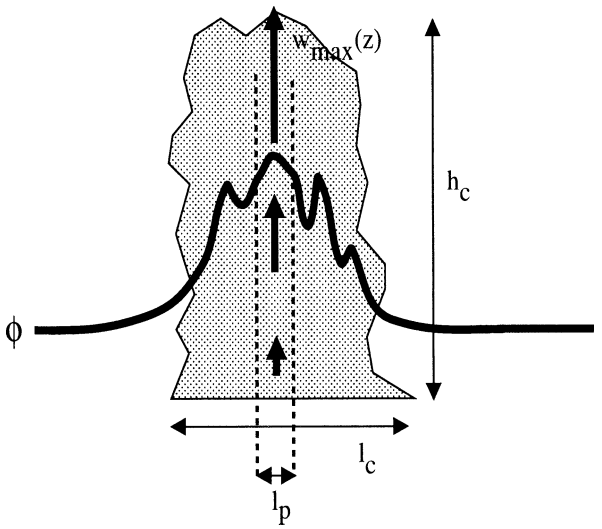

FIG. 3. Schematic vertical cross section through a cumulus cloud, illustrating the concept of a small parcel of a size l_p much smaller than the horizontal size l_c of the typical so-called top-hat anomaly in ϕ (temperature or moisture) associated with the cloud over the passive environment. To scale the turnover time of a parcel, the ratio is calculated of cloud depth h_c and the vertical velocity of the strongest updraft in the cloud $w_{\max}(z)$ (thick arrows) averaged along its path.

$$w_{\max,c} = \frac{1}{h_c}\int_{z_{0,c}}^{z_{0,c}+h_c} \max_{x,y}\,[w(x, y, z) - w(x, y, z_{0,c})]\,dz. \quad (10)$$

We average the vertical velocity along the path of the strongest updraft in the three-dimensional w field of the cloud. Therefore, the ratio of cloud depth h_c and this average maximum velocity $w_{\max,c}$ gives an estimate of the time the strongest updraft needs in order to rise from cloud base to cloud top, given the sampled velocity field of the cloud. Accordingly, the turnover timescale τ_c of the strongest updraft in the cloud is defined as

$$\tau_c \equiv \frac{h_c}{w_{\max,c}}. \quad (11)$$

Cumulus clouds root in the subcloud layer as thermals, and consequently they already have a vertical velocity at cloud base. The turnover time of the thermal at that point is the height above the surface divided by its vertical velocity in the subcloud layer. Accordingly τ_c is nonzero at cloud base. In the calculation of the τ_c of LES clouds we used the height of the cloud h_c as the length scale, which can be interpreted as the vertical extent of the whole thermal (cloud + subcloud part) corrected with cloud-base height. Therefore, to meet the boundary condition of a nonzero τ_c at cloud base, the vertical velocity should also be corrected with its cloud-base value, as is formulated in (10).

Many individual cumulus clouds are sampled in LES

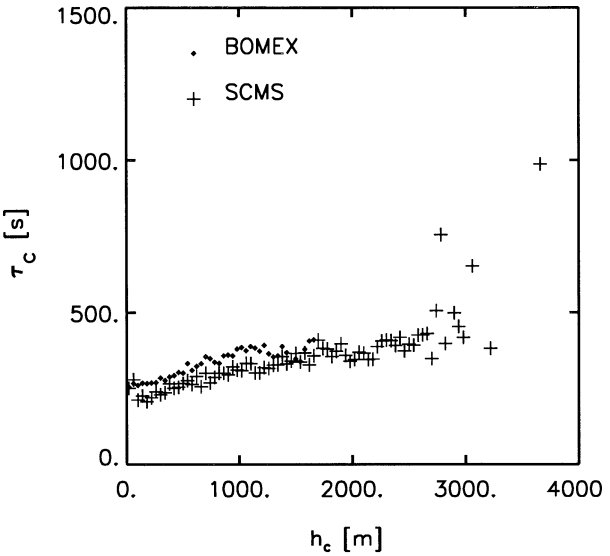

FIG. 4. A histogram of the average turnover timescale τ_c per cloud depth h_c as defined in (11). BOMEX is marked by diamonds, and SCMS by crosses. This figure is based on approximately 60 000 independent clouds per case, simulated with LES. The vertical resolution used in these simulations was 40 m. More detailed information on these simulations can be found in the appendix. Note that the number of clouds per bin typically decreases with cloud depth in a shallow cumulus ensemble, causing a lower quality of the statistics for the larger values of h_c.

for their $w_{\max,c}$ and h_c. To this purpose the instantaneous 3D liquid water field and vertical velocity field of each cloud at a certain moment are sampled. By using instantaneous fields we have no information on the stage of life of the clouds at the moment of sampling: they can still rise further or stop rising and dissipate. Nevertheless, by sampling enough independent, instantaneous clouds of all possible sizes and life stages, we get an effective relation between the depth of a cloud and the average vertical velocity of its strongest in-cloud updraft. After sampling many clouds this converged in a well-defined relation (see Fig. 4). It demonstrates that despite a small increase with cloud depth, τ_c is approximately constant for all clouds in both the BOMEX and the SCMS case. This has some important implications for the mixing rate of a parcel with its environment, as will be discussed later.

The turnover time τ_c in Fig. 4 is about 300 s, and is much smaller than the typical lifetime of real cumulus clouds, which is observed to be of the order 10^3 s. The reason for this is that clouds are continuously fed with air from the dry subcloud layer for some time, as the cloud is just the visible part of a thermal that is rooted in the subcloud layer and which can exist for some time. That determines the real lifetime of a cumulus cloud, and is therefore not equivalent to the turnover time of a single updraft parcel as defined here. The dilution timescale τ_p is taken proportional to the turnover timescale τ_c, using a dimensionless constant of calibration η. Substituting (9) into (8) and neglecting IV and V gives for $\phi \in \{\theta_l, q_t\}$

$$\frac{\partial \phi_p}{\partial z} = -\frac{\eta}{\tau_c w_p}(\phi_p - \overline{\phi}). \tag{12}$$

The same mechanisms of mixing are assumed for w_p. This is not a conserved property, and forcings have to be considered. We assume that the forcing in the vertical velocity budget of a rising parcel is dominated by the buoyancy term. The vertical velocity equation then consists of three terms, an advection term, a buoyancy forcing term and a dilution term. Furthermore, with $\overline{w} = 0$ we get

$$\frac{\partial w_p}{\partial z} = -\frac{\eta}{\tau_c} + \frac{B_p}{w_p}, \tag{13}$$

in which B_p is the buoyancy forcing,

$$B_p = \frac{g}{\theta_0}(\theta_v^p - \overline{\theta_v}). \tag{14}$$

Since the virtual potential temperature θ_v is a function of q_t and θ_l via the liquid water content q_l, (12) and (13) are coupled. Equations (12)–(14) together form the parcel model, which predicts the change of θ_l, q_t, and w of a parcel with height.

c. Discussion of the model

In many cloud and plume models the mixing (or entrainment) process is described as

$$\frac{\partial \phi_p}{\partial z} = -\epsilon(\phi_p - \overline{\phi}) \tag{15}$$

(Betts 1975; Anthes 1977; Tiedtke 1989; Raga et al. 1990). Equation (15) is a simple balance between vertical advection and lateral mixing. The fractional entrainment rate ϵ is the intensity of mixing and has the dimension m^{-1}, and could be interpreted as the inverse of the vertical mixing depth in which the excess of the rising element is diluted with an equal mass of environmental air. As a first-order approach it is often taken constant, but comparing (15) to (12), instead of a constant ϵ we propose

$$\epsilon = \frac{\eta}{\tau_c}\frac{1}{w_p} \sim \frac{1}{w_p}. \tag{16}$$

Assuming a constant ϵ means that the turnover timescale τ_c is inversely proportional to the vertical velocity scale of the eddy. In other words, the constant mixing depth would be reached in less time by faster parcels, but the intensity of mixing per vertical meter would be constant. However, the definition of τ_c in (11) used in this model appeared to be approximately constant in LES (see Fig. 4). This means that ϵ is not constant but is lower for higher vertical velocities, implying a larger mixing depth. This relation should be interpreted as follows:

the parcel rising faster through a layer with thickness Δz is spending less time in it, and has less time to interact with the surrounding air.

The w_p^{-1} relation in (16) represents a feedback between the mixing rate and the vertical velocity of the rising parcel. When buoyant parcels gain vertical velocity, their entrainment rate is decreased. It therefore can accelerate further, again decreasing its entrainment, and so on. This mechanism tends to make fast parcels entrain less than slow parcels, and therefore can be responsible for creating the large variability observed in Fig. 1. A constant entrainment rate would imply an essentially different mixing behavior without any feedback with the dynamics. The nature of this feedback mechanism will be discussed in more detail in the numerical results.

Similarly we can rewrite the vertical velocity equation (13) in a more familiar format, by substituting the new formulation (16) for the entrainment rate ϵ:

$$\frac{1}{2}\frac{\partial w_p^2}{\partial z} = -\epsilon w_p^2 + B_p, \tag{17}$$

(Simpson and Wiggert 1969; Gregory 2001). It demonstrates how buoyancy is transferred into kinetic energy.

4. A multiparcel approach

a. An ensemble of parcels

Most operational convection schemes in GCMs are bulk models in the sense that they use a single fractional entrainment rate ϵ, representative for a *whole* cloud ensemble. In contrast to those bulk parameterizations, this model is valid for just one small rising volume of air. By releasing a whole distribution of those parcels with slightly differing initial thermodynamic states, it is attempted here to reproduce the profiles and variability of θ_l, q_t, and w of a shallow cumulus cloud ensemble. The objective is to reproduce the cloudy tail in the conserved variable diagram in Fig. 1.

In the previous section it is attempted to find an expression for the mixing rate of a single parcel by using LES results to close the model, which resulted in the dynamical feedback in the mixing rate. All parcels in the ensemble have to obey the same budget equations (12)–(14). Consequently, each parcel will have a unique entrainment rate only dependent on its own vertical velocity, which in turn is dependent on buoyancy as a function of its conserved variables. Therefore, the variability in the parcel ensemble is only caused by the slightly differing initial conditions having a big impact higher up in the cloud layer.

There are similarities between this multiparcel model and the scheme of Arakawa and Schubert (1974); every element (or subensemble) in a cumulus cloud field has its own typical mixing rate. However there are also some major differences. In the Arakawa–Schubert scheme, a subensemble represents all clouds of a certain radius. The mixing rate of a subensemble is inversely proportional to its typical radius but constant with height. In contrast, this parcel model is formulated for just one small volume of air with constant area much smaller than a cloud, with a dynamical feedback in the mixing rate, which is therefore *not* constant with height.

b. Initialization and validation with LES

It is interesting to apply the multiparcel model to a convective boundary layer that is buoyancy driven from below by surface fluxes. In order to study the behavior of the model, it is validated with LES model results of shallow cumulus based on data from BOMEX and SCMS (see appendix A). As stated before, a whole ensemble of slightly different parcels is to be released, so initial distributions of the modeled variables θ_l, q_t, and w are needed for initialization. Because it is known from LES that so-called cloud core elements (elements that are both oversaturated and buoyant) are responsible for most of the vertical turbulent transport, it is interesting to compare the model with those elements. Therefore the validation of the model is limited to the cloud layer only, and the parcel ensemble is initialized at the level of maximum fractional core cover (LMC) which is always located close to cloud base in a shallow cumulus regime. The initial distributions at LMC are obtained from instantaneous fields of an LES simulation. The same number of parcels were initialized as there were LES grid boxes in the cloud core at LMC. The fractional core cover a_c (the ratio between cloud core area and total area) can also be calculated for the modeled ensemble at every level in the cloud layer, it being equal to the number of remaining parcels divided by the total number of grid points in the horizontal LES slice. In the BOMEX case, about 3% of all 128^2 LES grid points at LMC belonged to the cloud core. For SCMS this was about 4%.

For all parcels in the initial ensemble, the properties q_t, θ_l, and w are integrated upward from LMC using (12)–(14). The integration stops when a parcel stops rising. For $\overline{\phi}$ in (12) we use the horizontally averaged profiles of LES. An explicit finite-difference scheme is used for the vertical integration. An all-or-nothing condensation scheme is used to calculate the liquid water content $q_{l,p}$ needed in (14). For further numerical details of the scheme, see appendix B. At each height, properties of the modeled parcels that are still buoyant and oversaturated are compared to the cloud core of a horizontal LES slice.

The value of τ_c in (16) might be case dependent, depending on stability and other properties of the environment in which the clouds rise. But most importantly, τ_c is approximately constant for all clouds in each case. This results in a totally new conceptual model, for a feedback with the dynamics is now introduced in the entrainment rate. Our main goal is to create a model

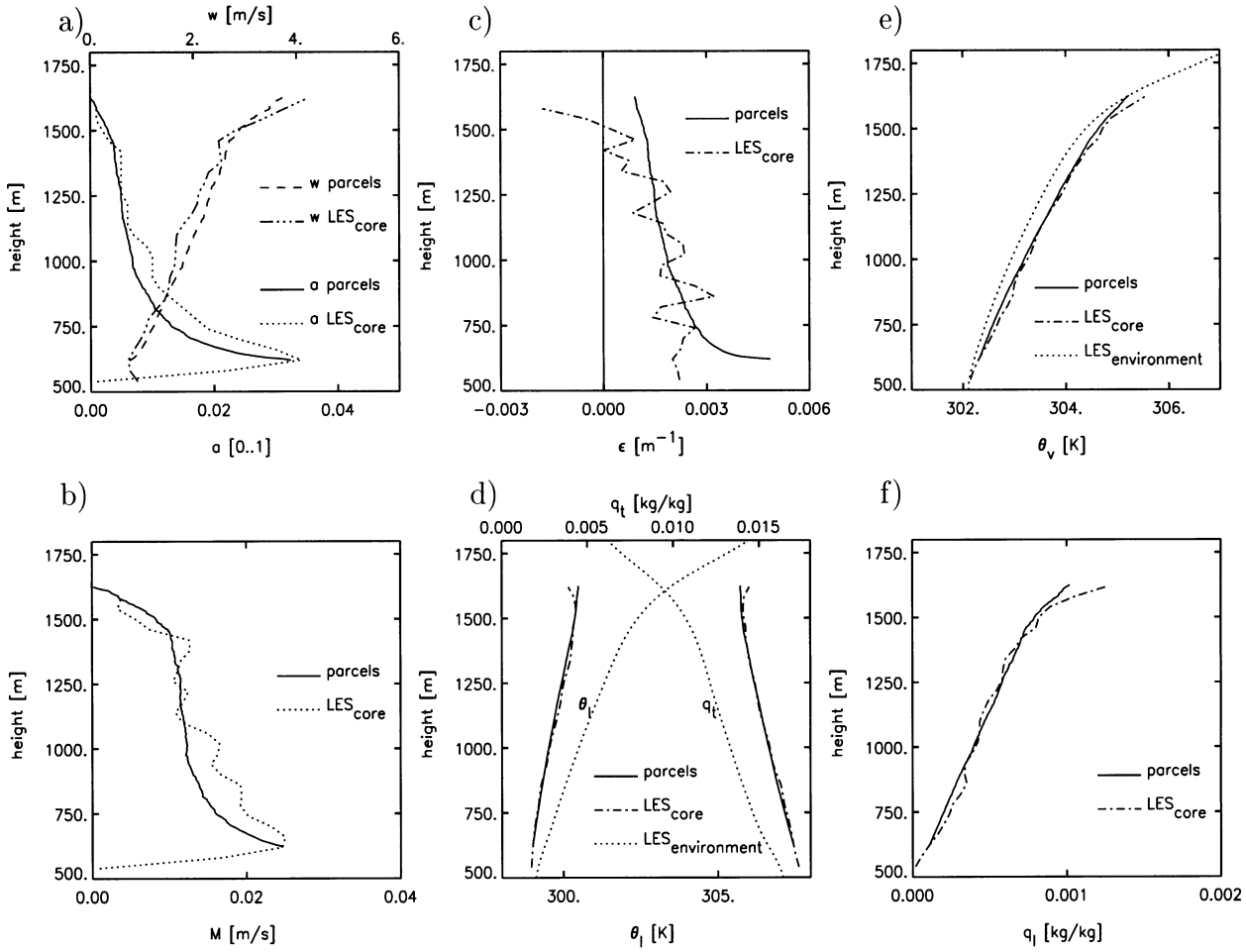

FIG. 5. Dynamical properties of the core of the parcel ensemble and LES for the BOMEX case (for details see appendix A). (a) The fractional cover a and vertical velocity w. (b) The mass-flux M. (c) The fractional entrainment rate ϵ. (d) The conserved variables θ_l and q_t. (e) Virtual potential temperature θ_v. (f) Liquid water content q_l. The label *core* denotes the average over the cloud core, and the label *environment* stands for the horizontally averaged environmental profile of LES. LES stands for the LES results, and parcels for the results of the modeled parcel ensemble.

that captures this important feedback, and therefore there is no sense in pinpointing an exact value for the turnover time at this point. For τ_c we take 300 s. The proportionality constant η is considered as a calibration factor here to obtain the optimum results. The value $\eta = 0.9$ is used for BOMEX, and $\eta = 1.2$ for SCMS. The results are presented in the next section.

5. Numerical results

a. Profiles

Every parcel reaches a height where the mixing (sink) term becomes larger than the buoyancy (source) term in (13), so that the right-hand side becomes negative and the parcel starts to decelerate. Eventually it falls out of the core (by definition) when it reaches zero buoyancy. Many parcels of initially different properties are released from cloud base, and as the elevation above cloud base increases, only the initially stronger parcels remain buoyant and oversaturated, causing the decreasing fractional core cover a_c with height (the subscript c stands for core) (see Figs. 5a and 6a). The functional relation of the mixing rate with the vertical dynamics makes the number of modeled core parcels decrease reasonably with height for BOMEX, but somewhat too fast for SCMS in the lower half of the cloud layer.

Figure 5a also shows the approximately linearly increasing w_c with height. The product $a_c \times w_c$ is the core massflux M_c, which looks quite promising in the sense that it is in the same order of magnitude as LES, and that it decreases with height (see Fig. 5b). This is not trivial because M_c is a product of two profiles, one increasing and one decreasing with height, making it sensitive to small changes. The fact that M_c decreases in the right order for BOMEX indicates that the modeled ensemble contains the changing dynamical properties of the LES core. For SCMS, the combination of a too low a_c and a too high w_c results in a local minimum in the

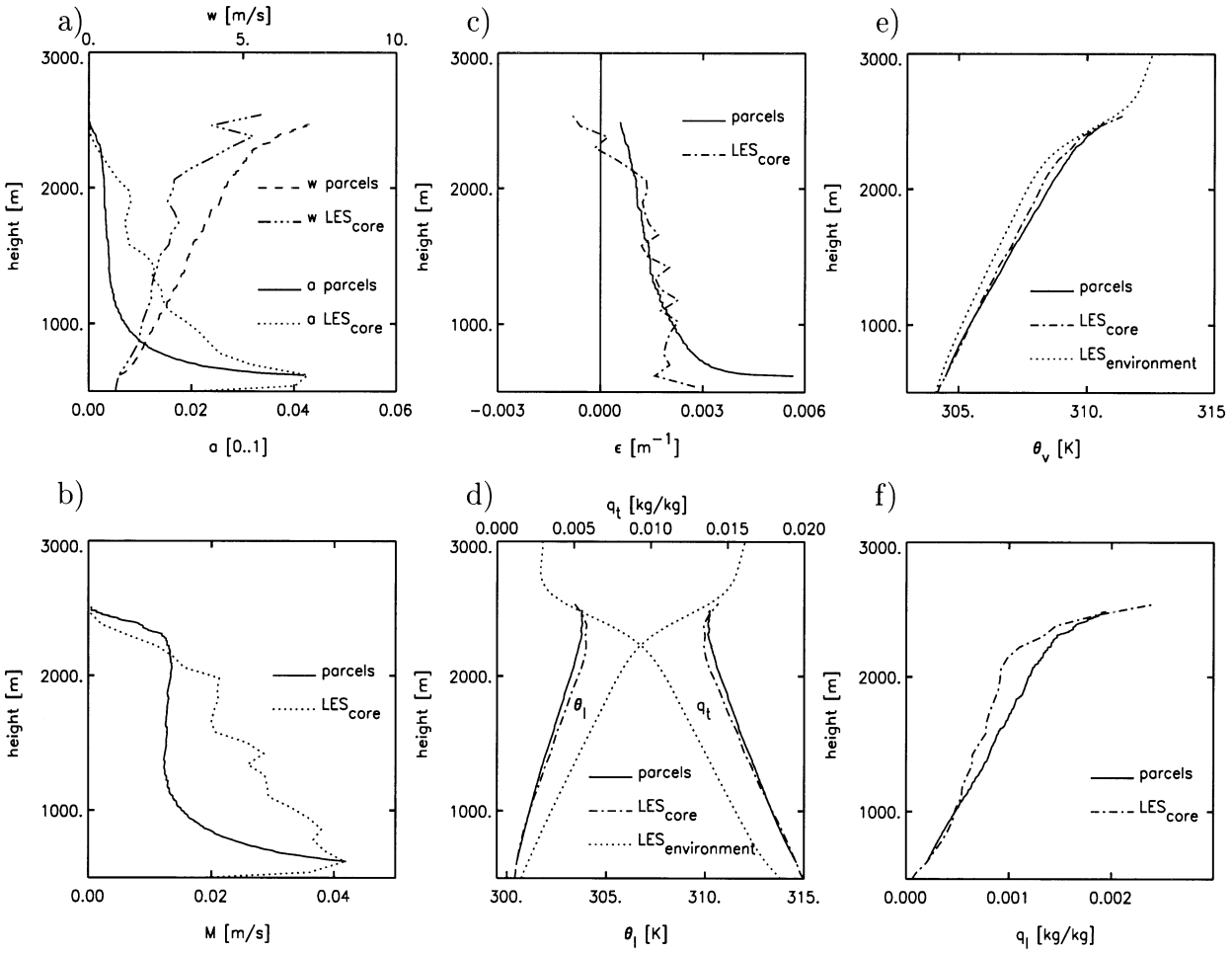

FIG. 6. Same as Fig. 5 but now for the SCMS case. For more details of this case see appendix A.

mass flux in the middle of the cloud layer (see Fig. 6b), which was not observed in LES.

The core-average entrainment rate ϵ_c of the parcel ensemble is calculated with

$$\epsilon_{c,\text{parcels}} = \frac{1}{N}\sum_{i=1}^{N} \epsilon_i, \tag{18}$$

where ϵ_i is the entrainment rate of an individual parcel, and N is the number of buoyant, oversaturated parcels at that height. Note that every average of the parcel ensemble is calculated with this method. In contrast, ϵ_c in LES is calculated indirectly, with the help of (15):

$$\epsilon_{c,\text{LES}} = \frac{-\dfrac{\partial \phi_c}{\partial z}}{(\phi_c - \overline{\phi})} \tag{19}$$

(see Betts 1975; Anthes 1977; Tiedtke 1989; Raga et al. 1990). This definition does not necessarily yield a positive value. Despite the different method of calculation, $\epsilon_{c,\text{parcels}}$ matches $\epsilon_{c,\text{LES}}$ in the bulk of the cloud layer (see Figs. 5c and 6c). Apparently the dynamical feedback in the entrainment rate of the individual parcels works good enough to create a distribution of entrainment rates of which the average is close to $\epsilon_{c,\text{LES}}$. In previous stochastic models, these distributions of mixing rates were often imposed (Raymond and Blyth 1986; Kain and Fritsch 1990; Emanuel 1991; Hu 1997), while here it changes with height dependent on the changing dynamics. The parameterizations of Grant and Brown (1999) and Nordeng (1994) do introduce feedbacks in the entrainment rate, but they describe a whole cloud ensemble at once and are not stochastic.

Only close to cloud base and the inversion do the entrainment profiles of LES and the parcel ensemble differ, which is just a result of the different method of calculation. In the trade wind inversion the vertical derivatives of the LES core average θ_l and q_t suddenly change sign, see Figs. 5d and 6d, implying a negative ϵ_c when calculated with (19). This feature in the q_t and θ_l profiles is reproduced by the parcel ensemble, and therefore represents a statistical result of the sudden removal of weaker parcels from the ensemble by the stability of the inversion. By this the core averages be-

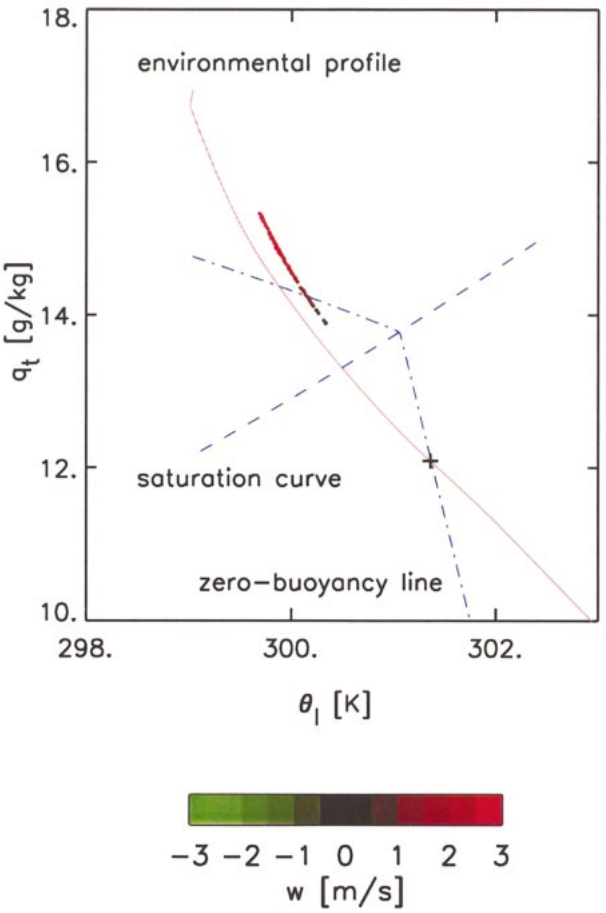

FIG. 7. The same conserved variable diagram as in Fig. 1 but now for the parcel ensemble.

come dominated by the few remaining parcels, which stayed more or less undiluted during their ascent from cloud base.

The parcel ensemble can maintain the marginally buoyant state of the cloud core until the inversion for BOMEX (see Fig. 5e). Comparing Fig. 5a to Fig. 5f, we see that the LES liquid water content and the core-top height are both reproduced. Figure 6e demonstrates that in the SCMS case the modeled core is too buoyant. Also, the excess of the core-average-conserved variables is too large (Fig. 6d), and too much liquid water is predicted (Fig. 6f). Too many weak parcels drop out of the ensemble too soon in the ascent from cloud base, and only a few undiluted ones remain that are responsible for the overestimated core-average vertical velocity, buoyancy, and liquid water, and also the minimum in the mass flux in the middle of the cloud layer, which is unrealistic.

b. Variability

Figure 7 shows a conserved variable diagram of the parcel ensemble for the BOMEX case. It can be directly compared to Fig. 1. The multiparcel model predicts enough parcels in the cloud core at this height (see Fig. 5a), they are located at the same location as the tail formed by the LES core grid points, and the parcel ensemble also shows the high correlation between q_t and θ_l as observed in LES. This result illustrates that the variability of the cloud ensemble can be understood by the stochastic application of this parcel model. The model is able to predict the thermodynamic variables of the strongest updrafts in the typical cloud-core tail of a conserved variable diagram of an LES cumulus cloud field.

In the model, the dynamical feedback in the entrainment rate is responsible for this. The vertical velocity feedback causes faster parcels to entrain less than slower parcels. So the q_t and θ_l of the former do not change much, while the latter are diluted heavily toward the environmental values, and the distributions of q_t and θ_l of the cloud core get wider with height (see Fig. 8). In this model, the passive environment ϕ is the only entrainment source for a parcel [see (12)], causing the modeled cloud tail to be narrower than LES. In reality (and LES) there are many more possible sources, like passive cloud air, downdraft air (Jonas 1990), and air from neighboring cloud points.

This increase of the width of the cloud-core distributions with height in the modeled parcel ensemble is determined by the intensity of the dynamical feedback in the mixing rate. This process is demonstrated in Fig. 8. Two different simulations are shown, one with a constant entrainment rate ϵ for all parcels and one with a constant turnover timescale τ_c. In case of a constant τ_c, the width of the LES cloud-core distributions increases with height from LMC, where it is still very small. The increase with height is somewhat too slow, but the shapes of the profiles are at least similar to LES. In contrast, the variance even decreases with height when a constant ϵ is used, independent of its value. In that case the parcels stay together without scattering much. Therefore, the dynamical feedback is responsible for the increasing variability of the cloud core with height.

6. Conclusions and perspectives

In this study, an expression for the lateral entrainment rate of a small updraft parcel is presented. The mixing terms in the parcel budget equations are written in a relaxation form, using a typical timescale that appears to be nearly independent of cloud depth in LES. This interesting result introduces a coupling between the entrainment rate and the dynamics of the parcel, in that faster parcels have a lower intensity of mixing. This makes the mixing process sensitive to the changing properties of the parcel as it rises.

These budget equations for a single parcel are applied to a whole ensemble of small updraft parcels. Every parcel is modeled individually, and thus it has its own unique entrainment rate, completely determined by its

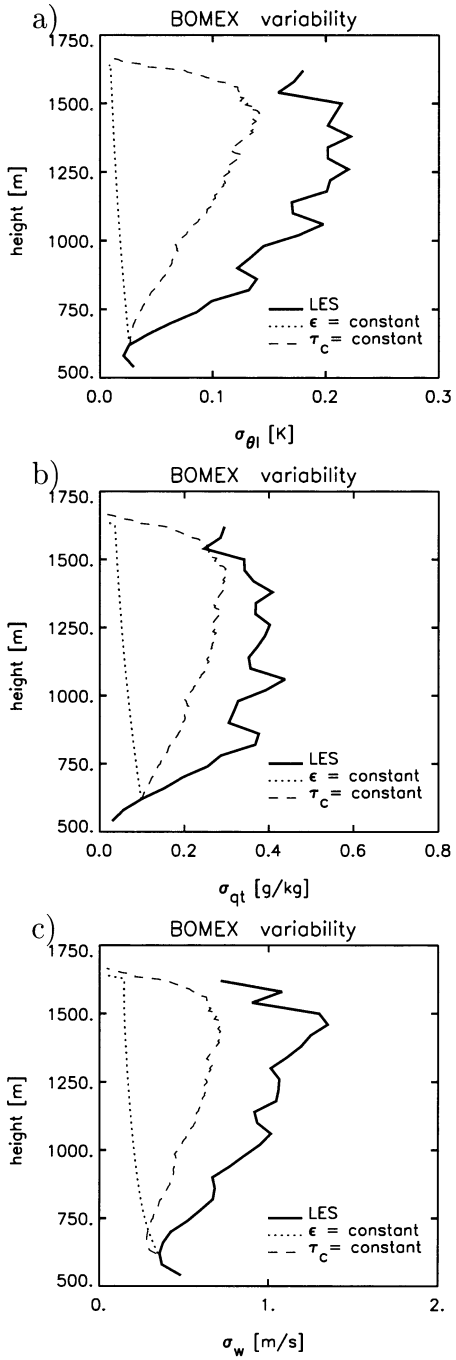

FIG. 8. The standard deviation of (a) θ_l, (b) q_t, and (c) w of the core ensemble around the core average for BOMEX. The spikiness in the LES profile is caused by the fact that an instantaneous 3D field is used for the validation.

vertical velocity. Therefore, the problem of finding the distribution of entrainment rates in the parcel ensemble is reduced to finding the initial distributions of the model variables at the level of initialization. In this evaluation, the parcel model is validated against LES results. Both the decreasing fractional cover and the increasing liquid water content with height of the LES cloud core were reproduced, as well as the vertical dynamics and mass flux, the core-average conserved variables, and the marginally buoyant state. The fractional entrainment rate of the parcel ensemble is always of the order of 10^{-3} m^{-1}, a value found by Siebesma and Cuijpers (1995) and Grant and Brown (1999) based on LES results.

The parcel model predicts the thermodynamic variables of the strongest updrafts in the cloud-core tail of a conserved variable diagram. The high correlation and the increasing variability with height of the characteristic cloudy tail found in LES conserved variable diagrams were also reproduced by the evaluation. It demonstrates that the typical variability of the cloud ensemble can be understood by the multiparcel model presented here. With knowledge of the variability, the total distributions of the conserved thermodynamic variables at one level in the cloud layer can be reconstructed. These can be used in statistical cloud schemes in GCMs to parameterize total cloud cover (Sommeria and Deardorff 1977; Cuijpers and Bechtold 1995).

What exactly causes the shortcomings in the SCMS case is yet unclear. Because the entrainment rate is dependent on the vertical velocity of the parcel, the model becomes sensitive for the vertical momentum equation. Here a very simple budget equation (13) is used. But in contrast to the thermodynamic variables, vertical momentum in clouds does not show a clear top-hat average over the passive environment (Fig. 3). This is due to the high incloud variability of vertical momentum and the occurrence of downdrafts inside the cloud. The LES results on the SCMS case indeed show vigorous convection featuring strong saturated downdrafts. Second, other forcings like pressure perturbations and molecular dissipation that can act as a sink for the vertical momentum in clouds, are not included in the model for simplicity. Thus the relaxation term represents all dilution processes in the w_p budget. We expect that a more sophisticated vertical momentum equation will improve the SCMS results.

In this experiment the model is validated on an LES cloud layer only, and the parcel ensemble is initialized at LMC, in order to keep the validation procedure as simple and clear as possible. But the rising thermals represented by the cloud core originate in the dry subcloud layer. Whenever a large dry thermal is strong enough to reach saturation and get positive buoyancy, it becomes an active cumulus cloud. If we assume that the functional relation for the entrainment rate, as found here for the cloud layer, is the same in the dry subcloud layer, then we can extend the model downward to the level where these large thermals originate, that is the surface layer (Businger and Oncley 1990; Wyngaard and Moeng 1992). By this the cloud layer gets linked to the subcloud layer, and the parcel ensemble then represents the upward transport in the whole boundary layer by all thermals starting at the top of the surface layer. The problem of finding the initial distributions is then moved

from LMC to this level. In this experiment we used distributions obtained from an LES simulation. To become completely independent of LES, joint Gaussian distributions at this level can be constructed (Wyngaard and Moeng 1992) using surface layer similarity theory (Holtslag and Moeng 1991). Such a rising parcel ensemble is interesting for use in convection schemes in GCMs because it can give the heights of the cloud base and top, and the fields of the strongest updrafts. This information is needed to close mass-flux convection schemes (Siebesma 1996; Tiedtke 1989). Work in this direction is still in progress.

The approximately constant turnover timescale resulting from LES is essential for the character of the parcel model, because it directly leads to the dynamical feedback in the entrainment rate. LES is still a model, and observational data can and should be used as well to determine the behavior of this turnover timescale for real clouds. The depth and maximum velocity of individual clouds should be known for this. At second, a qualitative validation of the parcel model in the form of a stochastic test with observational data requires in-cloud measurements of high resolution: it is necessary to have measurements of the vertical profiles of the environmental moisture and temperature, the heights of cloud base and top, and the distributions at enough levels in the cloud layer of temperature, moisture, and vertical velocity. The combination of these observations is scarce, especially if the observational data of the (initial) distributions form a problem. This is the reason to use LES fields instead for this study, but we are pursuing suitable observations to test the model with. The SCMS case has some potential because in-cloud measurements of turbulence by aircraft are available for this case, in combination with rawinsonde profiles and LandSat satellite images.

The lateral inflow term I and the turbulent mixing term II in the budget equations for a small in-cloud parcel were parameterized together in one relaxation formula, because no detailed information is available to determine which of the two terms dominates in this situation. Nevertheless it is interesting to study the nature of these two terms, especially for parcels of larger dimensions that may represent cloud-average fields. Historically, the boundary average ϕ_b in term I was often parameterized using an upstream method (Asai and Kasahara 1967; Tiedtke 1989): replacing ϕ_b by $\overline{\phi}$ in case of inflow (acceleration) gives the formula for the entrainment rate of a whole cloud ensemble as formulated by Nordeng (1994), which is currently being tested in the ECMWF model. Bulk models of this kind can be used to simulate the behavior of cloud-average fields, and their potential use lies in the application in convection schemes.

Acknowledgments. We thank Aad van Ulden, Geert Lenderink, and Bert Holtslag for many discussions on this subject. Peter Duynkerke kindly provided the SCMS data used in this study. The LES results in this study were obtained using the supercomputer facilities of the European Centre for Medium-Range Weather Forecasts (ECMWF) in Reading, United Kingdom. We thank three anonymous reviewers for their comments, which significantly improved this paper. This study has been supported by the Netherlands Organization for Scientific Research under Grant 750.198.06.

APPENDIX A

Shallow Cumulus Cases

Two shallow cumulus cases are used in this study to close and validate the stochastic model. The Barbados Oceanographic and Meteorological Experiment is described by (Holland and Rasmusson 1973). Another extensive description of this case can be found in Siebesma and Cuijpers (1995). The setup and results of the GCSS Working Group I intercomparison on this case in 1996 for both LES and 1D models can be found in Siebesma et al. (2001, manuscript submitted to *J. Atmos. Sci.*) and online at http://www.knmi.nl/~siebesma/bomex.html. In the BOMEX cumulus clouds over sea were studied. The LES case is made steady state by balancing the vertical turbulent transport by the large-scale forcings. Another shallow cumulus case is the Small Cumulus Microphysics Study, which took place in 1995 near Cocoa Beach, Florida. In this case the microphysics and variability of cumulus clouds over land were studied. It is a nonsteady-state case with a deepening cloud layer in time, with more vigorous cumulus convection than the BOMEX case. The initial mean profiles of θ_l and q_t of these two cases are shown in Fig. A1. Directly above the surface there is a well-mixed layer with a rather constant q_t and θ_l, followed by a conditionally unstable cloud layer and capped by a strong, stable inversion. SCMS is both warmer and moister in the well-mixed layer, and also has a deeper cloud layer of about two kilometers. These two different cumulus cases are chosen to critically test the stochastic parcel model under different circumstances.

To close the model, many LES clouds were sampled for their depth and maximum vertical velocity (see Fig. 4). A detailed description of the LES model used here can be found in Cuijpers and Duynkerke (1993). The BOMEX simulations consisted of a volume of dimensions $6.4 \times 6.4 \times 3.0$ km containing $128 \times 128 \times 75$ grid boxes, using a time step of 2 s. Five simulations of 8 h were performed, of which the last 5 h were used to sample all clouds in the volume at every 5 min. This is considered to be a sampling rate low enough for two subsequent sampled cloud fields to be independent of each other. This resulted in about 60 000 sampled clouds. For the SCMS case a volume of $6.4 \times 6.4 \times 5.0$ km was simulated with $128 \times 128 \times 125$ grid boxes. A smaller time step of 1 s had to be used in order to prevent numerical instability due to the large vertical

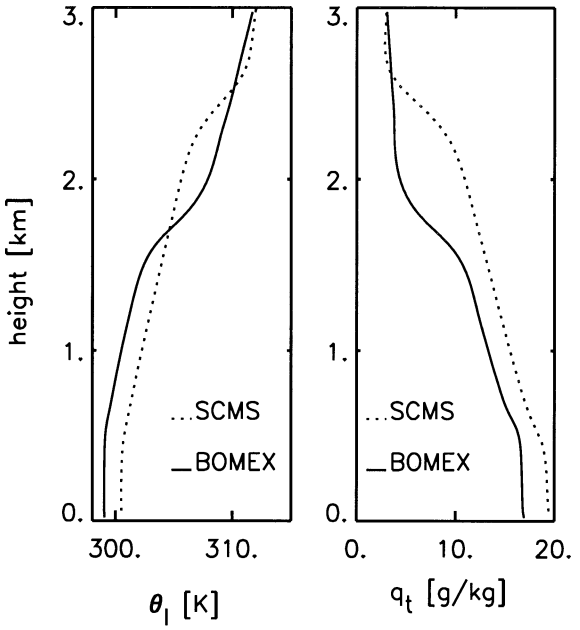

FIG. A1. Vertical profiles of the conserved variables of the BOMEX and SCMS cases, obtained from LES.

velocities in this case. The same sampling rate of 5 min was used. For the validation of the stochastic parcel model in section 5, randomly chosen instantaneous 3D LES fields of one of these simulations are used.

APPENDIX B

Numerics

To handle the set of coupled equations (12)–(14) numerically, we used an explicit finite-difference scheme on a staggered grid with w_p on the half levels and the conserved variables q_t and θ_l on the full levels. Equation (12) then becomes

$$\phi_{p,k+1} = \phi_{p,k} - \Delta z\left(\frac{\eta}{\tau_c}\frac{1}{w_{p,k}}\right)(\phi_{p,k} - \overline{\phi}_k), \quad \text{(B1)}$$

where $w_{p,k}$ is obtained by linear interpolation between the half levels $k + 1/2$ and $k - 1/2$. It is obvious that in order to integrate $\phi_{p,k}$, we have to know w_p at these two half levels. So w_p is integrated first to half level $k + 1/2$, being a function of buoyancy and vertical velocity at half level $k - 1/2$ only,

$$(w_{p,k+(1/2)})^2 = (w_{p,k-(1/2)})^2 - 2\Delta z\left(\frac{\eta}{\tau_c}w_{p,k-(1/2)} - B_{p,k-(1/2)}\right). \quad \text{(B2)}$$

Then the entrainment ϵ can be calculated on the full level k, by which we finally can integrate q_t and θ_l upward to $k + 1$. Liquid water q_l is calculated as a function of q_t, θ_l and pressure with an all-or-nothing condensation scheme, which means that the air within a parcel can only be entirely oversaturated or entirely undersaturated. We used an equidistant grid with a small vertical spacing of 5 m to minimize numerical errors.

REFERENCES

Anthes, R. A., 1977: A cumulus parameterization scheme utilizing a one-dimensional cloud model. *Mon. Wea. Rev.,* **105,** 270–286.

Arakawa, A., and W. H. Schubert, 1974: Interaction of a cumulus cloud ensemble with the large-scale environment. Part I. *J. Atmos. Sci.,* **31,** 674–701.

Asai, T., and A. Kasahara, 1967: A theoretical study of the compensating downward motions associated with cumulus clouds. *J. Atmos. Sci.,* **24,** 487–496.

Austin, P. H., M. B. Baker, A. M. Blyth, and J. B. Jensen, 1985: Small-scale variability in warm continental cumulus clouds. *J. Atmos. Sci.,* **42,** 1123–1138.

Beniston, M. G., and G. Sommeria, 1981: Use of a detailed planetary boundary layer model for parameterization purposes. *J. Atmos. Sci.,* **38,** 780–797.

Betts, A. K., 1975: Parametric interpretation of trade-wind cumulus budget studies. *J. Atmos. Sci.,* **32,** 1934–1945.

Blyth, A. M., 1993: Entrainment in cumulus clouds. *J. Appl. Meteor.,* **32,** 626–641.

——, W. A. Cooper, and J. B. Jensen, 1988: A study of the source of entrained air in Montana cumuli. *J. Atmos. Sci.,* **45,** 3944–3964.

Boatman, J. F., and A. H. Auer Jr., 1983: The role of cloud top entrainment in cumulus clouds. *J. Atmos. Sci.,* **40,** 1517–1534.

Brown, A. R., and Coauthors, 2001: Large-eddy simulation of the diurnal cycle of shallow cumulus convection over land. *Quart. Joy. Roy. Meteor. Soc.,* in press.

Businger, J. A., and S. P. Oncley, 1990: Flux measurement and conditional sampling. *J. Atmos. Oceanic Technol.,* **7,** 349–352.

Cuijpers, J. W. M., and P. G. Duynkerke, 1993: Large-eddy simulation of trade-wind cumulus clouds. *J. Atmos. Sci.,* **50,** 3894–3908.

——, and P. Bechtold, 1995: A simple parameterization of cloud water related variables for use in boundary layer models. *J. Atmos. Sci.,* **52,** 2486–2490.

Emanuel, K. A., 1991: A scheme for representing cumulus convection in large-scale models. *J. Atmos. Sci.,* **48,** 2313–2335.

Grant, A. L. M., and A. R. Brown, 1999: A similarity hypothesis for shallow cumulus transports. *Quart. J. Roy. Meteor. Soc.,* **125,** 1913–1936.

Gregory, D., 2001: Estimation of entrainment rate in simple models of convective clouds. *Quart. J. Roy. Meteor. Soc.,* **127,** 53–71.

Heymsfield, A. J., P. N. Johnson, and J. E. Dye, 1978: Observations of moist adiabatic ascent in northeast Colorado cumulus clouds. *J. Atmos. Sci.,* **35,** 1689–1703.

Holland, J. Z., and E. M. Rasmusson, 1973: Measurement of atmospheric mass, energy and momentum budgets over a 500-kilometer square of tropical ocean. *Mon. Wea. Rev.,* **101,** 44–55.

Holtslag, A. A. M., and C.-H. Moeng, 1991: Eddy diffusivity and countergradient transport in the convective atmospheric boundary layer. *J. Atmos. Sci.,* **48,** 1690–1698.

Hu, Q., 1997: A cumulus parameterization based on a cloud model of intermittently rising thermals. *J. Atmos. Sci.,* **54,** 2292–2307.

Jensen, J. B., P. H. Austin, M. B. Baker, and A. M. Blyth, 1985: Turbulent mixing, spectral evolution and dynamics in a warm cumulus cloud. *J. Atmos. Sci.,* **42,** 173–192.

Jonas, P. R., 1990: Observations of cumulus cloud entrainment. *Atmos. Res.,* **25,** 105–127.

Kain, J. S., and J. M. Fritsch, 1990: A one-dimensional entraining/detraining plume model and its application in convective parameterizations. *J. Atmos. Sci.,* **47,** 2784–2802.

Klaassen, G. P., and T. L. Clark, 1985: Dynamics of the cloud–environment interface and entrainment in small cumuli: Two-di-

mensional simulations in the absence of ambient shear. *J. Atmos. Sci.,* **42,** 2621–2642.
Lamontagne, R. G., and J. W. Telford, 1983: Cloud top mixing in small cumuli. *J. Atmos. Sci.,* **40,** 2148–2156.
Lin, C., and A. Arakawa, 1997: The macroscopic entrainment processes of simulated cumulus ensemble. Part I: Entrainment sources. *J. Atmos. Sci.,* **54,** 1027–1043.
Nordeng, T. E., 1994: Extended versions of the convective parametrization scheme at ECMWF and their impact on the mean and transient activity of the model in Tropics. ECMWF Tech. Memo. 206. [Available from ECMWF, Shinfield Park, Reading, RG2 9AX, United Kingdom.]
Paluch, I. R., 1979: The entrainment of air in Colorado cumuli. *J. Atmos. Sci.,* **36,** 2467–2478.
Pontikis, C., A. Rigaud, and E. Hicks, 1987: Entrainment and mixing as related to the microphysical properties of shallow warm cumulus clouds. *J. Atmos. Sci.,* **44,** 2150–2165.
Raga, G. B., J. B. Jensen, and M. B. Baker, 1990: Characteristics of cumulus band clouds off the coast of Hawaii. *J. Atmos. Sci.,* **47,** 338–355.
Raymond, D. J., and M. H. Wilkening, 1982: Flow and mixing in New Mexico mountain cumuli. *J. Atmos. Sci.,* **39,** 2211–2228.
——, and A. M. Blyth, 1986: A stochastic model for nonprecipitating cumulus clouds. *J. Atmos. Sci.,* **43,** 2708–2718.
Siebesma, A. P., 1996: On the massflux approach for atmospheric convection. *Proc. on New Insights and Approaches to Convective Parametrization,* Shinfield Park, Reading, United Kingdom, ECMWF.
——, 1998: Shallow cumulus convection. *Buoyant Convection in Geophysical Flows,* E. J. Plate, et al., Eds., Kluwer Academic, 441–486.
——, and J. W. M. Cuijpers, 1995: Evaluation of parametric assumptions for shallow cumulus convection. *J. Atmos. Sci.,* **52,** 650–666.
——, and A. A. M. Holtslag, 1996: Model impacts of entrainment and detrainment in shallow cumulus convection. *J. Atmos. Sci.,* **53,** 2354–2364.
Simpson, J., 1971: On cumulus entrainment and one-dimensional models. *J. Atmos. Sci.,* **28,** 449–455.
——, and V. Wiggert, 1969: Models of precipitating cumulus towers. *Mon. Wea. Rev.,* **97,** 471–489.
——, R. H. D. Simpson, A. Andrews, and M. A. Eaton, 1965: Experimental cumulus dynamics. *Rev. Geophys.,* **3,** 387–431.
Sommeria, G., 1976: Three-dimensional simulation of turbulent processes in an undisturbed trade-wind boundary layer. *J. Atmos. Sci.,* **33,** 216–241.
——, and J. W. Deardorff, 1977: Subgrid-scale condensation in models of nonprecipitating clouds. *J. Atmos. Sci.,* **34,** 344–355.
Squires, P., and J. S. Turner, 1962: An entraining jet model for cumulonimbus updraughts. *Tellus,* **14,** 422–434.
Stevens, B., and Coauthors, 2001: Simulations of trade wind cumuli under a strong inversion. *J. Atmos. Sci.,* **58,** 1870–1891.
Stommel, H., 1947: Entrainment of air into a cumulus cloud. *J. Meteor.,* **4,** 91–94.
Taylor, B. R., and M. B. Baker, 1991: Entrainment and detrainment in cumulus clouds. *J. Atmos. Sci.,* **48,** 112–121.
Tiedtke, M., 1989: A comprehensive mass flux scheme for cumulus parameterization in large-scale models. *Mon. Wea. Rev.,* **117,** 1779–1800.
Warner, J., 1970: On steady-state one-dimensional models of cumulus convection. *J. Atmos. Sci.,* **27,** 1035–1040.
——, 1977: Time variation of updraft and water content in small cumulus clouds. *J. Atmos. Sci.,* **34,** 1306–1312.
Wyngaard, J. C., and C.-H. Moeng, 1992: Parameterizing turbulent diffusion through the joint probability density. *Bound.-Layer Meteor.,* **60,** 1–13.